COMPUTER SIMULATION OF ACTION POTENTIAL PROPAGATION IN SEPTATED NERVE FIBERS

JOHN P. BARACH AND JOHN P. WIKSWO, JR.
Department of Physics and Astronomy, Vanderbilt University, Nashville, Tennessee 37235

ABSTRACT The nonlinear, core-conductor model of action potential propagation down axisymmetric nerve fibers is adapted for an implicit, numerical simulation by computer solution of the differential equations. The calculation allows a septum to be inserted in the model fiber; the thin, passive septum is characterized by series resistance R_{sz} and shunt resistance R_{ss} to the grounded bath. If R_{sz} is too large or R_{ss} too small, the signal fails to propagate through the septum. Plots of the action potential profiles for various axial positions are obtained and show distortions due to the presence of the septum. A simple linear model, developed from these simulations, relates propagation delay through the septum and the preseptal risetime to R_{sz} and R_{ss}. This model agrees with the simulations for a wide range of parameters and allows estimation of R_{sz} and R_{ss} from measured propagation delays at the septum. Plots of the axial current as a function of both time and position demonstrate how the presence of the septum can cause prominent local reversals of the current. This result, not previously described, suggests that extracellular magnetic measurements of cellular action currents could be useful in the biophysical study of septated fibers.

INTRODUCTION

Here we describe a computer simulation of action potential propagation down an idealized axon with a single transverse septum that is both thin and passive. The motivation for this work is the study of septa in the giant axons of the crayfish and earthworm and the associated perturbations in impulse propagation. In our work we do not attempt to match exactly the physiology of either animal but do try to use the observations of particular phenomena to set reasonable values for the parameters used in our core-conductor theory. In the earthworm, for example, Brink and Barr (1977) showed septa to be 50–300 μm apart in axons with a 96-μm diameter. By taking measurements at locations for which the axial voltage gradient inside the cell matched that outside in the bath, they found the axial (z-direction) septal resistance R_{sz} to be 38 kΩ. With an axoplasmic resistivity of 2.2 Ωm and a septal specific resistance R_s of $\sim 6 \times 10^{-4}\ \Omega m^2$, one can expect an axial septal resistivity of $\sim 10^5\ \Omega$m, about 2,000 times less than the membrane value. The septa vary from being slanted at ~150 degrees to the axial or z-direction, to being perpendicular to it. Electron microscopic inspection showed that these septa are made up of a small fraction (~5% by area) of junctional membrane that probably carries the axial currents (Brink and Dewey, 1978). The delay of the action potential as it crosses the septum was ~100 μs. In the crayfish (Watanabe and Grundfest, 1961) similar septa interrupt the lateral giant axon with a radius of 50 μm and an internal axoplasmic resistivity of ~1 Ωm, the septa being inclined at ~160° and separated by ~500 μm. In this case the specific resistance R_m of the membrane was 0.3 Ωm^2, about 500 times the septal value R_s found by Brink and Barr (1977). The septal resistance R_{sz} was estimated to be 300 kΩ; the septal shunt resistance in the radial direction, R_{ss}, was 150 kΩ. It was observed that propagation along the axon was delayed at the septum by ~100–250 μs at room temperature. More recent studies show the delay to be <100 μs (Ramon and Zampighi, 1980). A pronounced early rise or "shoulder" in the postseptal action potential waveform was also observed.

The work reported here uses an implicit solution to the nonlinear cable equations similar to that developed by Heppner and Plonsey (1970) for study of propagation through cardiac intercalated discs. In that work both series and shunt resistances to the bath were modeled and a "region of cardiac firing" (transmission of impulse) was found. The methods used here have also been used by Moore et al. (1975) and Joyner et al. (1978) as applied to cardiac fibers. Goldstein and Rall (1974) have used somewhat different mathematical methods to examine the change in the shape of the nerve action potential upon propagation into regions of differing properties. The effects of discontinuities on cardiac propagation were examined by Sharp and Joyner (1980) and Joyner et al. (1984). The analysis we present examines the voltage and current distributions in septated nerves.

METHODS

In this model, we consider a long length of cylindrical, axially symmetric axon that is interrupted by a thin, passive, transverse septum. Because this is a one-dimensional analysis, we do not model effects associated with slanted septa. Fig. 1 shows the equivalent resistor model of the section of axon on either side of the septum. The axon is divided into 33 segments,

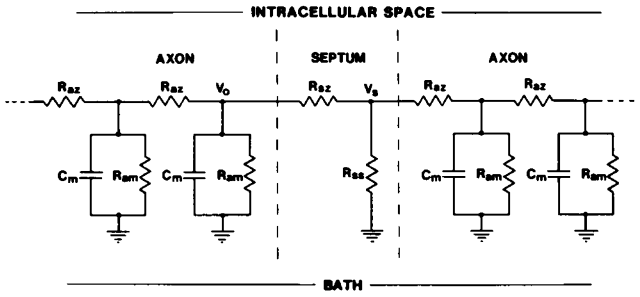

FIGURE 1 A simple model for a septated axon. R_{az} represents the septal series resistance and R_{ss} the septal shunt resistance to the grounded bath.

with the lumped parameters of the septum located between segments 15 and 16. Each axon segment is characterized by an axial resistance R_{az}, and a time- and voltage-dependent membrane conduction current obtained from the Hodgkin–Huxley equations (Scott, 1975). This nonlinear behavior of the axonal membrane could be described by a nonlinear membrane resistance R_{am}. The septum is characterized by an axial resistance R_{sz} and a shunt resistance R_{ss}. We assume that the bath is grounded, so that extracellular potentials are not included in the analysis. We can obtain an upper limit on the septal capacitance by assuming that the entire 50-μm radius septum has the 6-nm thickness of the nexus. In this case the septal capacitance would be 60 pF. If the septal capacitance was charged through the half-millimeter length of axon between the septa, the time constant for charging the septal capacitance would be ~7 μs. Since this time constant is much shorter than the action potential risetime and also shorter than the timesteps used in our calculation, we can ignore it. Moreover, the estimated upper limit for septal capacitance is equivalent to the axonal membrane capacitance of a length of ~0.02 mm, 10 times less than our space step. Accordingly, our model considers two regular space steps of axon, near the middle of the fiber, separated by a very thin, entirely passive septum of negligible capacitance. It is thus completely characterized, in this approximation, by series and parallel septal resistances.

As shown by Moore et al. (1975), an explicit numerical integration of the cable equations using the Hodgkin–Huxley equations for the membrane current J_g is difficult. The equations are nonlinear and vary strongly when the membrane current is large. As a result, calculations using the Runge–Kutta method described by Goldstein and Rall (1974) tend to be unstable and may diverge unless exceedingly small timesteps are used. A linearization of the membrane equations may be used (Drouhard and Roberge, 1982), but the implicit method of solution described by Joyner et al. (1978) is a more satisfactory approach for many cases and has been used in our calculations.

We consider a time t at which the transmembrane potential V is known and represents an action potential propagating in the positive z-direction and focus our attention on a single arbitrary position, z. The calculation of V as a function of t and z is based on the core-conductor model (Plonsey and Fleming, 1969). The development, beyond using the voltage laws for capacitors and resistors, amounts merely to writing the continuity equation for current. We have previously described the continuum differential equation for core-conductor models (Barach et al., 1985). In our present calculation, we interrupt a length of uniform axon at its midpoint by a lumped parameter septum, which we assume to have no spatial thickness. Thus the septum separates two spatial "steps" of the computer simulation and occupies no length, consistent with our approximation that the plane of the septum is perpendicular to the axis of the axon.

Since we will take a discrete step approach from the start, the intracellular current coming towards z from z-δz at some time t may be written as the current $I((z - 1/2\delta z),t)$ midway between z-δz and z. By Ohm's law, this current is the voltage difference $V(z - \delta z,t) - V(z, t)$, divided by the resistance, where δz is the space step between segments of axon. Following the approach of Moore et al. (1975), we in fact will compute the time average of this current over the interval between times t and $t + \delta t$

$$\langle I(z - 1/2\delta z)\rangle = 1/2[V(z - \delta z, t) - V(z, t) + V(z - \delta z, t + \delta t) - V(z, t + \delta t)]/R_{az} \quad (1)$$

where δt is the timestep used in the calculation. The axial resistance R_{az} is equal to $\rho\delta z/\pi a^2$, where a is the fiber radius and ρ is the axoplasmic resistivity.

The current arriving at the point z inside the axon may go four places: (a) Some may exit outward through the membrane as a conduction current density J_g. If the Hodgkin–Huxley equations are used to describe $J_g(V)$ as in Scott (1975), then the membrane conduction current I_g through the axon membrane resistance R_{am} may be calculated by multiplying J_g by the surface area of the segment

$$I_g(z) = 2\pi a J_g(V(z))\,\delta z. \quad (2)$$

(b) Some of the current arriving at z from the preseptal axon may charge the membrane capacitance. This capacitive current is determined by the time-derivative of the transmembrane voltage and the capacitance of the segment

$$\langle I_c(z)\rangle = C_m\, 2\pi a\delta z\, \frac{[V(z, t + \delta t) - V(z, t)]}{\delta t}, \quad (3)$$

where C_m is the membrane capacitance per unit area. (c) If a septum is present, some current that arrives at z may be diverted outward and flow radially through the shunt resistance R_{ss} to the grounded bath. This septal shunt current I_{ss} will have a time average given by the average voltage at the septum divided by the shunt resistance, i.e.,

$$\langle I_{ss}(z)\rangle = 1/2[V(z, t) + V(z, t + \delta t)]/R_{ss}. \quad (4)$$

Finally, (d) if the septum is present, some current may proceed down the fiber through the series septal resistance R_{sz} as well as R_{az} of the next segment of the axon. By Ohm's law, its time average is given by the voltage gradient across both the septum and the next segment, divided by the combined resistance of the septum and the segment

$$\langle I_{az}(z + 1/2\delta z)\rangle = 1/2[(V(z, t) - V(z + \delta z, t) + V(z, t + \delta t) - V(z + \delta z, t + \delta t)]/(R_{az} + R_{sz}). \quad (5)$$

Continuity of current requires that Eq. 1 equal the sum of Eqs. 2–5, thereby allowing us to eliminate all currents from the equations in favor of voltages. For convenience we multiply both sides of the equation by $2R_{az}$ and define the constants

$$A = 1/(1 + R_{sz}/R_{az}) \qquad B = R_{az}/R_{ss}$$
$$S = 4\rho\delta z^2/a \qquad W = C_m S/\delta t \quad (6)$$

We move all the terms referring to the later time, $t + \delta t$, to the left side of Eq. 5 to obtain

$$(W + 1 + B + A)V(z, t + \delta t) - AV(z + \delta z, t + \delta t) - V(z - \delta z, t + \delta t) = (W - 1 - B - A)V(z, t) + AV(z + \delta z, t) + V(z - \delta z, t) - SJ_g(V(z, t)). \quad (7)$$

In this equation we make the simplification of calculating J_g using the voltage at (z, t) rather than using a time average. Thus if small enough time and space steps are taken (determined by the stability of the results), the error is small. The timestep is set by the ratio of S to W. We choose to keep this ratio at unity so that for a C_m of 10^{-2} F/m^2, the timestep, δt, is 0.01 ms. In most calculations we set S to 2 Ωm^2, a to 50 μm, and ρ to 0.5

Ωm so that δz equals 0.22 mm and R_{az} is 14 kΩ. The ratio of δz to δt is 22 m/s, which gives an indication of the speed of the system.

Eq. 7 has three unknown voltages if all initial values at time t are given. The method of solution is to write a matrix equation from Eq. 7, in which the zeroth spatial position is the known stimulus voltage as a function of time, and the voltage at final position z_{n+1} is determined by requiring it to equal that at z_n, so that no current would flow out of the end of the axon. We solved this matrix equation with a BASIC computer program that used the MAT INV command on a DEC 1099 computer (Digital Equipment Corp., Marlboro, MA). The computation was limited to 33 spatial steps, which required a 33-by-33 matrix inversion.

RESULTS

Fig. 2 shows a typical set of propagating action potential waveforms calculated for positions z_{10}, z_{17}, and z_{22}, with the septum located between z_{15} and z_{16}, and where each spatial step corresponds to 0.22 mm. The traces have been shifted in time to align their peaks. The calculated membrane ionic current, $J_g(t)$, at z_{10} is also shown. Note that the membrane current remains small for approximately the first 200 μs after the corresponding transmembrane voltage trace begins to rise. This indicates that the early current is largely capacitive, as expected; the current signal also has the usual shape (Hobbie, 1978). The action potential has a calculated propagation velocity of 6.5 m/s for this choice of parameters. Increases in the peak sodium conductance $\bar{g}_{Na}$ in the calculation of $J_g(V)$ produce faster and steeper action potentials, as expected. These traces are similar to measured events for a variety of experimental preparations and have shapes expected from cable analysis (Barach et al., 1985). The waveform for z_{22}, 1.3 mm past the septum, is sufficiently beyond the influence of the septum that it appears quite similar to the z_{10} trace, with the same amplitude and late shape. Its early shape, from 100 μs onward, is similar to that at z_{10} with a somewhat steeper risetime and more gradual early "foot." The trace at z_{17} is immediately postseptal and displays a pronounced elevation from 0.1 to 0.4 ms as compared with the other two traces. This represents in our simulation the "shoulder" found prominently in crayfish action potentials (Wata- nabe and Grundfest, 1961), in which the closest postseptal electrode positions actually overlapped the long, slanted septum, in contrast to the transverse septum in our model. A similar effect is shown in Fig. 8 *b* of Heppner and Plonsey (1970) for rather different conditions.

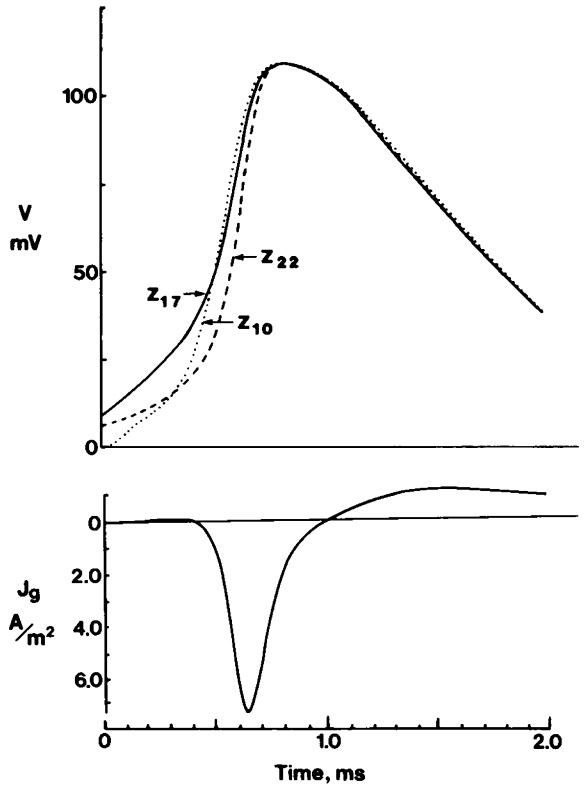

FIGURE 2 (*Top*) Three transmembrane potential waveforms at different positions along a septated axon, time-shifted so that the peak voltages align. *Dotted curve*, for Axial position z_{10}, 1.3 mm before the septum; *dashed curve*, z_{22}, 1.3 mm beyond the septum. They are approximately similar. *Solid curve*, z_{17} immediately postseptal, showing a noticeable early rise. R_{sz} and R_{ss} were both chosen to be 3.0 R_{az} for this simulation. (*Bottom*) Membrane current at z_{10}. Its early portion is close to zero, as expected, until threshold depolarization is reached at t = 0.3 ms.

The time and position dependence of V_m is shown in Fig. 3, *a* and *b* for an R_{sz} of 0.5 R_{az} and R_{ss} of 2.3 R_{az}. In Fig. 3 *a* the spatial variation of the voltage is shown as a collection of "snapshots" at sequential times. The septum at 3.5 mm is vividly evidenced by the notch in voltage. In Fig. 3 *b* the results are displayed with the time axis horizontal so that it is easy to visualize the time delay as the action potential propagates past the septum.

In the preseptal and postseptal regions, the time of the peak action potential increases linearly with distance along the axon. The septum introduces a delay that is evidenced in a plot of peak position versus time as an offset between two straight segments of the curve whose slopes correspond to the preseptal and postseptal conduction velocities. This offset is clearly evident in Fig. 3 *b*, for which the delay, Δt, is 0.5 ms.

It has recently been demonstrated that magnetic techniques can be used for quantitative determination of the axial intracellular current (Roth and Wikswo, 1985). In our model the axial current can be determined by dividing the spatial derivative of the potential by the appropriate axial resistance. It is important to realize that in the case of septated axons the conduction velocity is not constant, so it is not possible to use the temporal derivative of the voltage in lieu of the spatial derivative, as is usually done in the core conductor analysis of single uniform axons. Fig. 3, *c* and *d* shows the spatial and temporal dependence of the axial current from two perspectives. It is clear from this figure that as the action potential approaches the septum and the voltage is drawn down, the axial current rises steeply, as shown in Fig. 3 *c*, and becomes prolonged in time as shown in Fig. 3 *d*. As the action potential passes the septum, the transmembrane potential increases with distance along the postseptal axon, as shown in Fig. 3 *a*. Thus

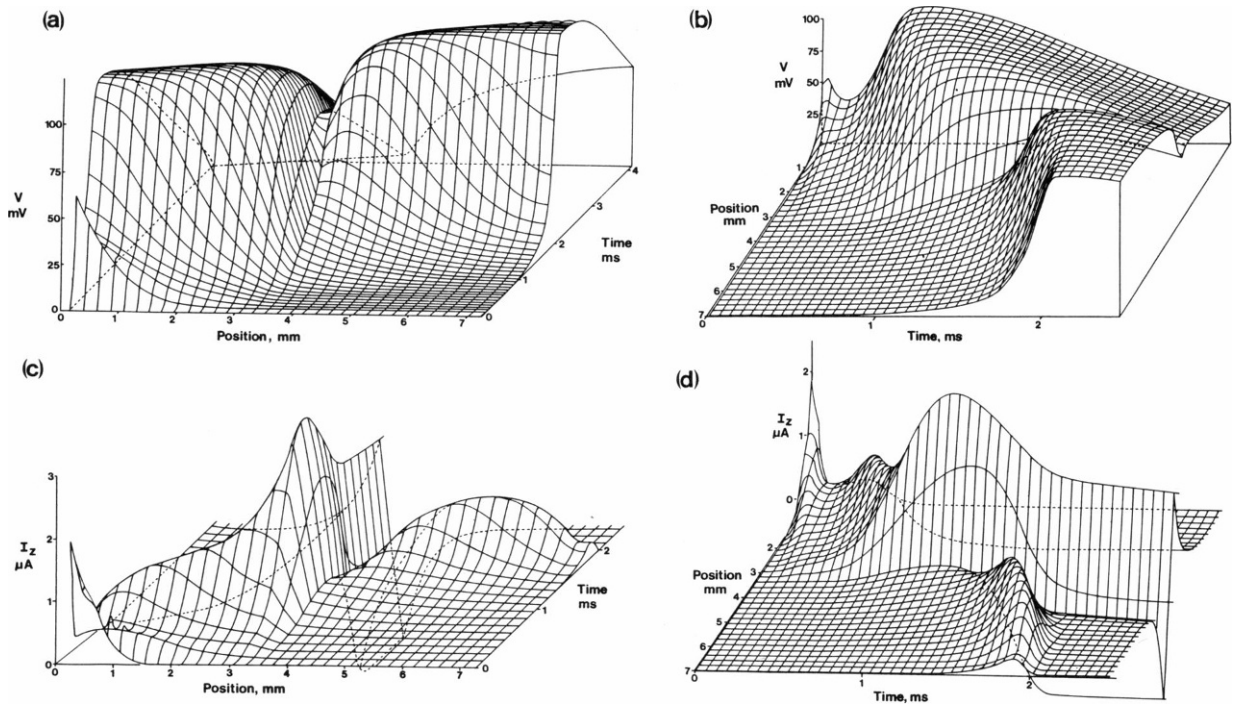

FIGURE 3 (*a* and *b*) Two isometric views of the surface that describe the spatial and temporal variation of the transmembrane action potential for a septated axon with R_{sz} equal to 0.5 R_{az} and R_{ss} equal to 2.3 R_{az}. The septum is at z = 3.4 mm. (*c* and *d*) Similar views showing the spatial and temporal dependence of the axial current in the septated nerve.

the spatial derivative of V is positive postseptally, whereas it was negative preseptally. For this reason, the postseptal axial current must have the opposite sign as compared with the preseptal axial current. This reversal of current is most evident in Fig. 3 *d*, and occurs for all times during the action potential in the postseptal positions adjacent to the septum. This effect can be viewed as the result of the septal shunt resistance draining current to the bath from both the preseptal and postseptal regions. As the action potential approaches the septum, this additional current drain increases the normally positive axial current. After the action potential crosses the septum, the depolarization current being shunted to the bath by the septum opposes the axial current normally associated with the action potential. In Fig. 3, *c* and *d* the shunt current is sufficiently large that the net axial current is negative in the immediate postseptal region.

ANALYSIS OF SEPTAL EFFECTS

Simulations for more than 40 choices of parameters were made and checked for stability. We found that use of either a $\bar{g}_{Na}$ four times greater than normal or a timestep three times greater than normal caused severe fluctuations in the calculated potential. We have investigated a range in R_{sz} from 0 to 10 R_{az}, and in R_{ss} from 12,000 R_{az} to 1.2 R_{az}, where 30 kΩ is a common value for R_{az}. These limits represent a vanishing septum, and a vanishing postseptal action potential, respectively. We have also examined solutions with $\bar{g}_{Na}$ ranging from 900 to 3,600 $\Omega^{-1}m^{-2}$ in addition to the usual value of 1,200 $\Omega^{-1}m^{-2}$ (Scott, 1975). (Other parameters left constant in these runs were $\bar{g}_K$ = 360 $\Omega^{-1}m^{-2}$, $\bar{g}_{leak}$ = 3 $\Omega^{-1}m^{-2}$. For our timesteps of 0.01 ms, m, the alpha coefficient for the fast Na^+ gate, is 0.001 and other coefficients are as in Scott, scaled as indicated.)

Delays Δt are observed to range from 0 to >1 ms; the latter representing a far more pronounced septal effect than observed in nature. The peak membrane voltage at the septum drops monotonically as R_{sz} increases and R_{ss} decreases, where both changes result in an increase in Δt. The maximum of the action potential is always smaller just preseptally at z_{15} than just postseptally at z_{16}. For example, when both R_{sz} and R_{ss} equal 3 R_{az}, Δt is 0.62 ms and the proximal voltage maximum is 66% of the voltage that would be recorded in a uniform axon without septa (termed the septum-free voltage V^*). The distal voltage is 71% of V^*. For an R_{sz} of 0.5 R_{az}, and R_{ss} of 20 R_{az}, the delay is 0.09 ms and the maxima are 95 and 96% of V^*, respectively.

We have tested the simple hypothesis that the observed delay in the traversal of the septum by the action potential is closely related to the potential change, ΔV, between V_s at the septum and V^*. The series resistance delays the voltage rise while the shunt resistance pulls the voltage V_s towards ground. Similarly, the rise in the postseptal voltage is impeded by the septum, further delaying the postseptal action potential until it moves free of the septum. To model these effects, we first note that during the time of rapid rise

in the membrane voltage, the membrane resistance is very low and R_{az} serves as the output impedance of a pre-septal current source. Referring to Fig. 1, we find that the septal voltage drop can be written in terms of the axial current I_{az} in the axon and the septal shunt current I_{ss}

$$\Delta V = I_{az}R_{sz} + I_{ss}R_{az}. \quad (8)$$

If the septum was non-existent, R_{sz} and I_{ss} would be zero so that ΔV would be zero. The shunt current I_{ss} is given by V_s/R_{ss}, and V_s is equal to the preseptal voltage V_0 minus $I_{az}R_{sz}$, so ΔV can be written as

$$\Delta V = I_{az}R_{sz}(1 - R_{az}/R_{ss}) + V_0R_{az}/R_{ss}. \quad (9)$$

Because increases in $\bar{g}_{Na}$ result in increased conduction velocities and, we assume, decreased delays, we would expect that Δt was inversely related to $\bar{g}_{Na}$. Since we assume that larger septal voltage drops will be associated with larger septal time delays, we hypothesize that the time delays can be explained by an equation that includes the features of Eq. 9 as well as the inverse dependence on sodium conductance:

$$\Delta t = (\alpha/R_{ss} + \beta R_{sz}(1 - R_{az}/R_{ss}))(1{,}200\ \Omega^{-1}\mathrm{m}^{-2}/\bar{g}_{Na})^{\gamma}, \quad (10)$$

where Δt is measured in milliseconds.

Delays observed in 57 simulations with different values of model parameters were used to obtain a set of values for α, β, and γ with minimum rms error in the fit (α = 1.1 ms $\times R_{az}$, β = 0.06 ms/R_{az}, γ = 0.75). These three parameters were then used to calculate the delays for each simulation using Eq. 10, with the observed and calculated delays plotted in Fig. 4 for each simulation. Reasonable agreement verifies our heuristic picture. When R_{ss} was less than 2 R_{az} or R_{sz} greater than 10 R_{az}, we found that the observed 1 ms or longer delays were larger than those predicted by Eq. 10, but since such long delays are not found in crayfish or earthworm axons, they were not included in Fig. 4. In the physiologically realistic range of delays of 0.06–0.60 ms, Eq. 10 and the voltage-loss model that inspired it appear to provide a reasonable and simple empirical description.

For fixed values of R_{sz} and R_{ss}, a fourfold variation in $\bar{g}_{Na}$ causes Δt to change by a factor of 3.1; a factor of 2.8 is predicted by Eq. 10 with the best value of γ = 0.75. This 10% discrepancy in Δt may arise either from limitations in our model or inaccuracies in the measurement of time differences for action potentials whose shapes vary along the axon.

Note that Eq. 10 gives a Δt of 0.5 ms for a small R_{sz} of 0.5 R_{az} and an R_{ss} of 2.3 R_{az} (the case shown in Fig. 2). The same value of Δt is obtained with R_{sz} and R_{ss} of 4 R_{az}, in which case the series impedance is eight times greater and the shunt resistance is almost doubled. That indicates that the septal conditions may be such that the same delay can occur in septa that range from being shunt dominated to being series dominated. We compare two cases in which the values of R_{ss} vary by a factor of 2 but a compensating variation in R_{sz} (from 0.1 to 5.0 R_{az}) produces the same Δt. Fig. 5 shows the leading edges of the action potential at preseptal and postseptal locations. In both cases the time delay measured at 70% of the peak amplitude of the action potential is ~0.35 ms. While the postseptal waveforms are similar, the preseptal action potential for the series-dominated case is larger and has a shorter risetime than the shunt-dominated case.

Since there are various values of R_{ss} and R_{sz} that give the same delay, an independent measure of the septal effects would allow us to separate the shunt and series contributions. The sharper preseptal waveform in Fig. 5 allows this. We measure the time for the action potential to rise from 18 to 71% of its maximum and call that time τ. (Since the maxima are reached very slowly for any septum that drastically affects propagation, this measure of the rapid portion of the rise is more reliable than would be the time to peak signal.) For an unseptated axon, we would

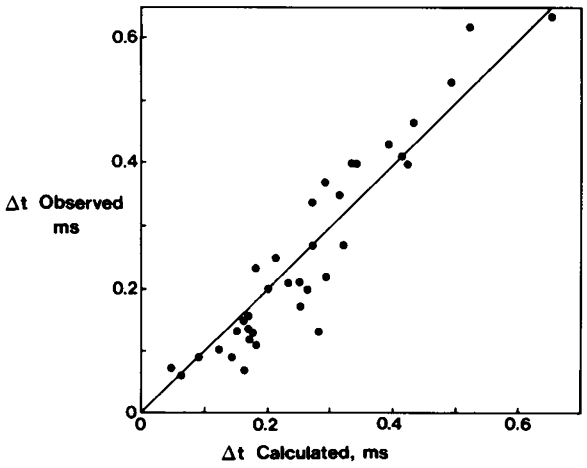

FIGURE 4 Comparison of simulation septal delays and those calculated using Eq. 10.

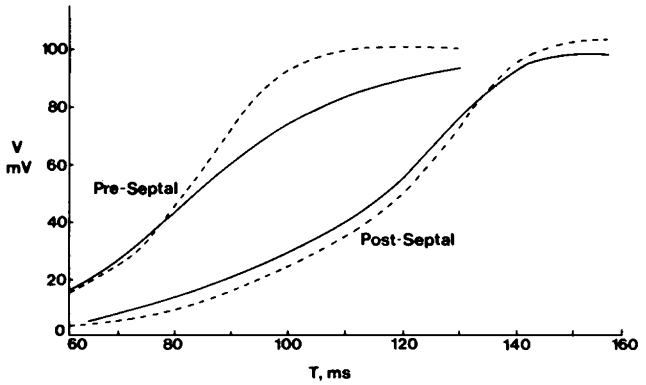

FIGURE 5 Comparison of action potentials at z_{14} (preseptal) and z_{17} (postseptal) positions for two different types of septa. *Dashed curves*, R_{sz} = 5.0 R_{az} and R_{ss} = 8.0 R_{az} (series dominated); *solid curves*, R_{sz} = 0.1 R_{az} and R_{ss} = 4.0 R_{az} (shunt dominated).

expect the time constant τ^* to be approximately proportional to $R_{az}C_m$, since the membrane is charged by the axial current originating from already depolarized membrane. For a position just before the septum, however, the current coming from the proximal side of the septum will be partially diverted out to the bath through the septal shunt resistance. As a result, the voltage at such a position, V_0, will rise more slowly than the voltage V^* at a septum-free location:

$$V_o = V^*(R_{sz} + R_{ss})/(R_{az} + R_{sz} + R_{ss}). \quad (11)$$

This reduction in the driving voltage should lead to a proportional increase in the risetime τ_0 just before the septum

$$\tau_o = [1 + R_{az}/(R_{sz} + R_{ss})]\tau^*. \quad (12)$$

From this, we expect that if either R_{sz} or R_{ss} is large, then τ_0 should equal τ^*, even though large R_{sz} produces a large Δt and a large R_{ss} produces a small Δt. This effect is shown in Table I where preseptal risetimes taken from the simulated action potentials are compared with those predicted by Eq. 12, using τ observed at z_{14} for τ_0. The risetime differences are small but striking when displayed for cases of equal Δt.

The combined use of Eqs. 10 and 12 should allow estimation of R_{sz} and R_{ss} from measurements of septal delay and preseptal risetime without the need for any direct impedance measurements. For example, if a particular septated axon had a septal delay of 0.34 ms and a preseptal action potential with risetime 19% longer than that found away from the septum, Eqs. 10 and 12 then could be used with best values for α, β, and γ and a $\bar{g}_{Na}$ of 1,200 $\Omega^{-1}m^{-2}$ to give estimates of R_{sz} of 1.3 R_{az} and R_{ss} of 4.0 R_{az}, i.e., a very shunt-dominated case.

These characterizations might be shown much more clearly in magnetic measurements of action currents, such as those of Wikswo et al. (1980), Barach et al. (1985), and Roth and Wikswo (1985). In such measurements the axial current peaks of Fig. 3, *c* and *d* would appear directly at positions near the septum. The size of these peaks is greater

TABLE I

Δt	$\frac{R_{sz}}{R_{az}}, \frac{R_{ss}}{R_{az}}$	τ Observed	τ Calculated
ms		*ms*	*ms*
0.33	0.1, 4.0	0.40	0.37
0.36	5.0, 8.0	0.35	0.34
0.44	1.0, 3.0	0.39	0.38
0.44	8.0, 8.0	0.30	0.32
0.54	0.5, 2.3	0.41	0.41
0.55	4.0, 4.0	0.35	0.34
0.74	1.0, 2.0	0.40	0.40
0.76	8.0, 4.0	0.33	0.33

the smaller the shunt resistance and they persist for a long time after the depolarization pulse has passed, as shown in Fig. 3. Indeed, the figure gives a graphic example of the importance of current measurements in non-uniform fiber systems. Voltage measurements made at any position naturally give V and its time derivative. In uniform systems this time derivative is directly proportional (through the velocity) to the space derivative represented by the current. In a system such as ours, however, the space and time derivatives are drastically different: indeed, at every space position the voltage merely rises monotonically during depolarization, whereas the currents at some positions rise and at others fall sharply.

The effects of the septum on the propagating action potential are also evident in the axial current waveforms shown in Fig. 3, *c* and *d*. Because of the septal shunt resistance, the axial current is always largest on either side of the septum. As we discussed before, the shunt resistance results in an additional axial current that is positive preseptally and negative postseptally, which will reduce or even reverse the net postseptal current. This additional current, which we will term ΔI_{az}, flows ohmically through the axial resistance R_{az} producing an additional axial voltage drop over that in the septum-free axon

$$\Delta I_{az}R_{az} = V^* - V_s = \Delta V. \quad (13)$$

Thus the additional axial voltage drop should increase as the shunt current increases. Fig. 6 shows a plot of the

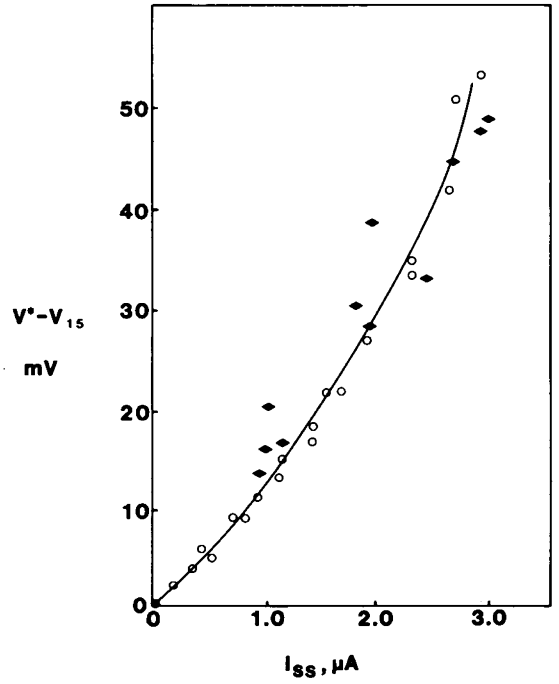

FIGURE 6 A plot of the septal voltage drop as a function of the shunt current through the septal shunt for 32 simulations covering two orders of magnitude variation in R_{ss}. *Diamonds*, R_{sz} values between 4.0 R_{az} and 11 R_{az}. *Circles*, R_{sz} between 0.1 R_{az} and 2.0 R_{az}.

preseptal voltage drop $V^* - V_{15}$ plotted as a function of the current through the septal shunt, which is V_{15}/R_{ss}.

DISCUSSION

We have presented a simple simulation of the propagation of action potentials in septated nerves. With this model we have explored the dependence of septal time delays and action potential risetimes for a range of septal properties, and we have presented a simple phenomenological explanation for these changes. One of the more interesting predictions of this analysis is the local reversal of axial current at the septum. In uniform axons that exhibit dispersionless propagation of the action potential with a velocity u, it is a standard technique to use spatial and temporal derivatives interchangeably since

$$dV/dz = 1/u\, dV/dt. \quad (14)$$

In septated nerves, however, these two derivatives are not equivalent everywhere because of the decreased action potential velocity at the septum. This effect is of little import on measurements of the transmembrane potential but may be extremely important in the direct, magnetic measurement of the axial current. Our simulation shows that at least for certain choices of septal resistances the perturbation of the septum is sufficiently large to result in local increases in preseptal current and correspondingly large reversals in the postseptal current. Since the present analysis is based upon the core conductor model, it is difficult, if not impossible, to predict the extent to which this local current perturbation will be manifest in the electric and magnetic fields at some distance from the axon. A more detailed analysis using a volume conductor model will be necessary to determine whether these effects can be observed with existing experimental techniques.

The authors thank Peter Brink, Frans Gielen, and Brad Roth for their detailed comments on this manuscript.

This work has been supported in part by National Institutes of Health grant 1-R01 NS-19794 and Office of Naval Research contract N00014-82-K-D107. Computer time has been provided by the College of Arts and Science, Vanderbilt University.

Received for publication 31 March 1986 and in final form 18 July 1986.

REFERENCES

Barach, J. P., B. J. Roth, and J. P. Wikswo, Jr. 1985. Magnetic measurements of action currents in a single nerve axon: a core-conductor model. *IEEE Trans. Biomed. Eng.* 32:136–140.

Brink, P., and L. Barr. 1977. Resistance of the septum of the giant axon of earthworm. *J. Gen. Physiol.* 69:517–536.

Brink, P., and M. M. Dewey. 1978. Nexal membrane permeability to anions. *J. Gen. Physiol.* 72:67–86.

Drouhard, J-P., and F. A. Roberge. 1982. Simulation of repolarization of cardiac Purkinje fiber action potential. *IEEE Trans. Biomed. Eng.* 29:481–490.

Goldstein, S. S., and W. Rall. 1974. Changes of action potential shape and velocity. *Biophys. J.* 14:731–757.

Heppner, D. B., and R. Plonsey. 1970. Simulation of electrical interaction of cardiac cells. *Biophys. J.* 10:1057–1075.

Hobbie, R. K. 1978. Intermediate Physics for Medicine and Biology. John Wiley & Sons, Inc., New York. Chapter 6.

Joyner, R. W., R. Veenstra, D. Rawling, and A. Chorro. 1984. Propagation through electrically coupled cells. *Biophys. J.* 45:1017–1025.

Joyner, R. W., M. Westerfield, J. W. Moore, and N. Stockbridge. 1978. Numerical methods of modeling excitable cells. *Biophys. J.* 22:155–170.

Moore, J. W., F. Ramon, and R. W. Joyner. 1975. Voltage clamp simulations I. Methods and tests. *Biophys. J.* 15:11–19.

Plonsey, R., and D. G. Fleming. 1969. Bioelectric Phenomena. McGraw-Hill Book Co., New York.

Ramon, F., and G. Zampighi. 1980. On the electrotonic coupling mechanism of crayfish segmented axons: temperature dependence at junctional conductance. *J. Membr. Biol.* 54:165–171.

Roth, B. J., and J. P. Wikswo, Jr. 1985. The magnetic field of a single axon. A comparison of theory and experiment. *Biophys. J.* 48: 93–109.

Scott, A. C. 1975. Electrophysics of a nerve fiber. *Rev. Mod. Phys.* 47:487–533.

Sharp, G. H., and R. W. Joyner. 1980. Simulated propagation of cardiac action potentials. *Biophys. J.* 31:403–424.

Watanabe, A., and H. Grundfest. 1961. Impulse propagation at septal junctions of crayfish axons. *J. Gen. Physiol.* 45: 267–308.

Wikswo, J. P., Jr., J. P. Barach, and J. A. Freeman. 1980. Magnetic field of a nerve impulse: first measurements. *Science (Wash. DC).* 208:53–55.